

Spectral-domain differential interference contrast microscopy

Yizheng Zhu,* Natan T. Shaked, Lisa L. Satterwhite, and Adam Wax

Department of Biomedical Engineering, Duke University, Durham, North Carolina 27708, USA

*Corresponding author: yizheng.zhu@duke.edu

Received October 6, 2010; revised December 7, 2010; accepted December 21, 2010;

posted January 11, 2011 (Doc. ID 136229); published January 31, 2011

We present a fiber-optic low-coherence imaging technique, termed spectral-domain differential interference contrast microscopy (SD-DIC), for quantitative DIC imaging of both reflective surfaces and transparent biological specimens. SD-DIC combines the common-path nature of a Nomarski DIC interferometer with the high sensitivity of spectral-domain low-coherence interferometry to obtain high-resolution, quantitative measurements of optical pathlength gradients from a single point on the sample. Full-field imaging can be achieved by scanning the sample. A reflected-light SD-DIC system was demonstrated using a USAF resolution target as the phase object. Live cardiomyocytes were also imaged, achieving a resolution of 36 pm for pathlength gradient measurements. The dynamics of cardiomyocyte contraction were recorded with high sensitivity at selected sites on the cells. © 2011 Optical Society of America

OCIS codes: 110.0180, 180.3170, 120.3180, 170.5810.

Since its advent in the 1950s, Nomarski differential interference contrast (DIC) microscopy has become one of the standard imaging modalities in modern optical microscopes and is widely used today in the imaging of live and unstained biological specimens [1]. Conventional DIC microscopy is inherently a qualitative technique due to the nonlinear relationship between the image intensity and the optical pathlength (OPL) gradient. Further, DIC images are biased by the intrinsic intensity variations within the sample. In recent years, quantitative DIC microscopy has received growing attention. A number of implementations have been proposed to isolate and quantify the OPL gradient of the sample from conventional DIC images [2–4]. From these gradient measurements, quantitative OPL or phase maps of the sample can be reconstructed [3,5]. In most of these systems, a partially coherent light source was used in order to reduce speckle noise, but its broadband nature has not been fully exploited.

On the other hand, spectral-domain low-coherence interferometry (SD-LCI), perhaps best exemplified by spectral-domain optical coherence tomography, has been used broadly and shown to have a sensitivity advantage over its time-domain counterparts [6]. When combined with common-path interferometry, SD-LCI can offer superior resolution in the measurement of pathlength or pathlength gradient [7–9].

In this Letter, we propose spectral-domain differential interference contrast (SD-DIC) microscopy. The SD-DIC technique combines the common-path nature of DIC microscopy with the high sensitivity of SD-LCI to produce high-resolution, quantitative measurement of the optical pathlength (OPL) gradient across a sample. We demonstrate SD-DIC imaging for both reflective objects (USAF resolution target) and transparent objects (live ventricular cardiomyocytes). Further, the dynamics of cardiomyocyte contraction were recorded at selected sites on the cells.

A schematic of the SD-DIC system is shown in Fig. 1(a). The output of a single-mode fiber-pigtailed superluminescent diode (Superlum, Inc.; $\lambda = 840$ nm, $\Delta\lambda = 40$ nm) is split equally using a polarization control-

ler into the slow and fast axes of a 32.5 cm polarization-maintaining (PM) fiber. The light is then collimated, and a Nomarski prism splits it into *o* and *e* waves. The PM fiber is rotated such that its axes are aligned with the *o* and *e* polarizations of the Nomarski prism. An objective (Carl Zeiss, Inc.: 40 \times ; 0.75) focuses both beams onto the sample with a slight lateral shear that is smaller than the size of a diffraction-limited spot. The sample is scanned in two dimensions using motorized actuators.

For applications such as surface profiling shown in Fig. 1(b), photons directly reflected by the sample surface are detected. For thin, relatively transparent samples such as cells, they are adhered to a reflective surface to enable double-pass transmission measurement, as illustrated in Fig. 1(c). A glass chamber may be used to keep cells alive in culture media. In both cases, reflected *o* and *e* waves travel back through the same optics to be mixed in the single-mode fiber to interfere. A polarization controller can be used to maximize the fringes. The interference signal is detected by a spectrometer (OceanOptics: HR4000).

Although the configuration in Fig. 1(a) is similar to a conventional reflected-light DIC microscope, the key difference that enables high-resolution spectral-domain operation is the PM fiber. It functions as a phase retarder and adds a large bias, 215 μ m one-way in this system, to

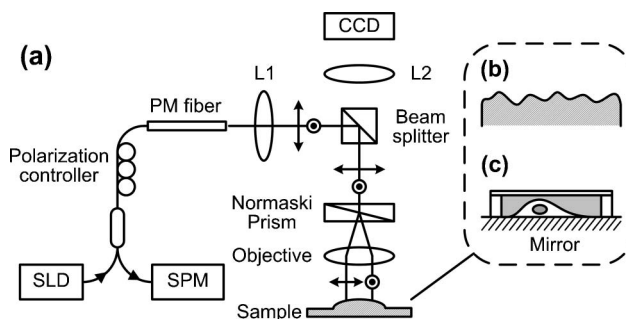


Fig. 1. SD-DIC system. (a) Schematic. SLD, superluminescence diode; SPM, spectrometer; L1 & L2, lenses. (b), (c) Possible sample configurations for surface profiling and live cell imaging, respectively.

the OPL gradient between the o and e waves. The detected intensity at the spectrometer is hence given by

$$I_t(k; x, y) \propto r_o^2(x, y) + r_e^2(x, y) + 2\eta r_o(x, y)r_e(x, y) \times \cos[2k(\Delta L_{PR} + \delta L_{NP} + \delta L_{DIC}(x, y))], \quad (1)$$

where r_o and r_e represent the reflectivities of a surface or the transmissivities of a cell at position (x, y) for the o and e waves, respectively; k is the wavenumber; η is the interference visibility; and ΔL_{PR} , δL_{NP} , and δL_{DIC} are one-way OPL differences generated by the phase retarder, the Nomarski prism, and the sample gradient, respectively.

Equation (1) shows that the phase retarder functions similarly to the frequency shifter in a heterodyne system. Without the phase bias, δL_{NP} and δL_{DIC} will result in only low-frequency interferometric modulation of the spectrum because of their submicrometer or nanometer magnitudes. Such modulation makes accurate phase determination difficult in the presence of DC background intensity and low-frequency noises. In contrast, these undesired signals can be effectively avoided with a large bias ΔL_{PR} , which shifts the interferometric signal to higher spectral frequency.

Once the interferogram is acquired, it is processed to extract the term $(\Delta L_{PR} + \delta L_{NP} + \delta L_{DIC})$ [7,8], where $(\Delta L_{PR} + \delta L_{NP})$ constitutes a background constant and δL_{DIC} represents the quantitative OPL gradient of the sample. In addition to accurate OPL measurement, the total intensity of the signal, obtained by the summation of $I_t(k; x, y)$ across the entire bandwidth, also provides us a close approximation of the bright-field (intensity) image, which represents the reflectivity or transmission distribution across the sample.

We first demonstrate the system using the chromium (Cr) pattern of a positive USAF resolution target (Edmund Optics). Figure 2(a) shows the δL_{DIC} image of Group 7, Element 1, where the width of each Cr bar is $3.9 \mu\text{m}$. The surface step between the Cr coating and the uncoated glass substrate provides DIC contrast and generates a clear shadow-cast appearance. The bright-field image, as the summation of $I_t(k; x, y)$, is shown in Fig. 2(b) for comparison. Cross-sectional profiles from both images are plotted in Figs. 2(c) and 2(d), respectively. In the DIC curve, the positive and negative peaks clearly indicate rising and falling edges. The unequal magnitudes suggest an oblique incident angle. The axial resolution of the δL_{DIC} measurement on the coated surface is 32 pm. The transverse resolution is $0.95 \mu\text{m}$, estimated from the 10%–90% edge response in the intensity curve.

An interesting observation is that the bars appear wider in the DIC image than in the bright-field image. As seen in the cross-sectional profiles in Figs. 2(c) and 2(d), the DIC peaks are not located exactly at the middle of the intensity slopes but rather shift toward the slope bottom. Hence the separation of the positive and negative peaks measures $5.0 \mu\text{m}$, which is greater than the $3.8 \mu\text{m}$ FWHM of the intensity peak (actual bar width $3.9 \mu\text{m}$). The $1.2 \mu\text{m}$ discrepancy results from the drastic contrast in reflectivity between the glass substrate and the Cr coating. As illustrated in Fig. 2(c) inset, even when

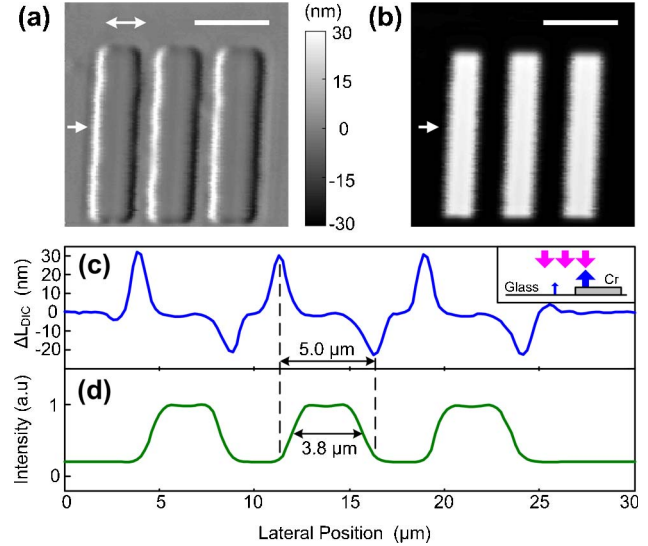


Fig. 2. (Color online) SD-DIC images of a USAF resolution target. (a), (b) OPL gradient and bright-field intensity images of Group 7, Element 1; double arrow indicates the shear direction; scale bar is $10 \mu\text{m}$. (c), (d) Cross-sectional profiles taken from (a) and (b) at positions indicated by the single arrows; inset explains the increased bar width in (a).

the beam incidents mostly on the glass, the reflected light and its OPL can be dominated by photons reflected by the coating, generating the illusion that the entire incident beam is already on the coated area and hence extending its size. This artifact is the result of the decoupling of phase and intensity in perhaps all quantitative DIC techniques but will manifest itself only where there is steep contrast in reflectance or transmittance. Under these circumstances, apparent transverse dimension in the phase image of an object may not reflect its actual size; but the intensity image will accurately carry such information and may be used together with the phase image to better characterize the object. Nevertheless, the OPL measurement is still highly accurate. In addition, this phenomenon is expected to have minimal practical significance for most biological samples of interest for this technique, since they do not exhibit steep changes in transmission.

Live cell imaging was also performed on the SD-DIC system. To prepare the sample, ventricular cardiomyocytes were isolated from two-day old Sprague Dawley rat neonates and cultured for 24 h on a reflective surface coated with human fibronectin [10].

Figures 3(a) and 3(b) show the OPL gradient and intensity images of an isolated cardiomyocyte. Although the intensity image has an artifact, appearing as a bright spot on the left side, it does not affect the DIC image. This immunity demonstrates the excellent decoupling of the OPL gradient from intensity using spectral-domain demodulation and signifies one of the important advantages of the proposed system.

To monitor live cell dynamics, the DIC signal at the circled spot in Fig. 3(a) was recorded for 120 s with a sampling rate of 83 Hz (limited by spectrometer speed). The top curves in Fig. 3(c) show that two pulsatile motion events were observed, each with a duration of 0.5 s. For comparison, a background signal was recorded

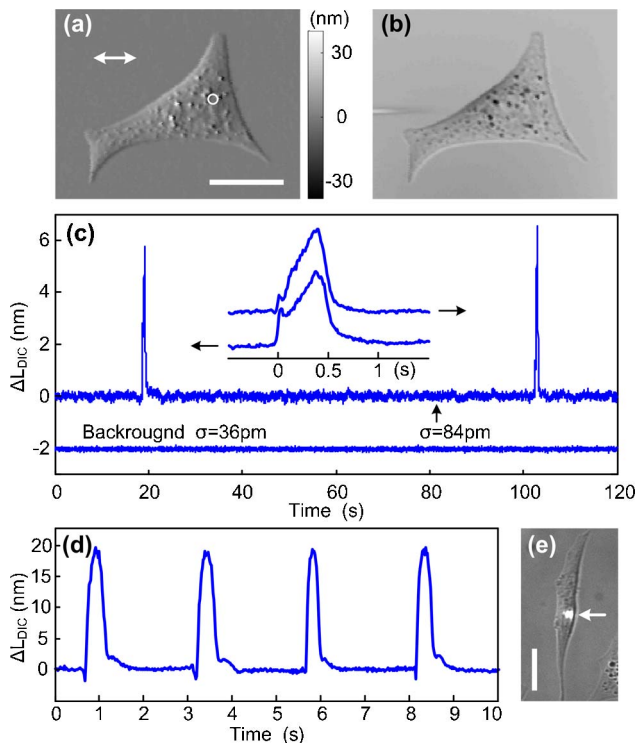


Fig. 3. (Color online) Live cardiomyocyte measurements. (a) OPL gradient image of an isolated cardiomyocyte; double arrow indicates shear direction. (b) Corresponding bright-field image. (c) Upper, stochastic beating events at the circle in (a) for 2 min; inset shows enlarged view of the two beating events; lower, background signal taken at the upper-left corner of the image. (d) Regular beating sequence of another cardiomyocyte shown in photograph (e), where the bright spot indicates illuminated location. Scale bars are $20\ \mu\text{m}$.

outside the cell, showing a resolution of 36 pm without averaging or filtering. This value is comparable to that obtained previously with the resolution target, although the beam now passes through the liquid culture medium. This is evidence of superior suppression of ambient fluctuations by the DIC common-path geometry. Figure 3(d) shows the dynamics of a second cardiomyocyte, registering four periodic beating events in 10 s with an average duration of 0.4 s.

We believe that the relatively rare events in the first cardiomyocyte are consistent with stochastic contractions often observed in freshly isolated ventricular cardiomyocytes, whereas the regular events in the second cardiomyocyte are of the same frequency as contraction

cycles observed in “pacing cells,” a type of specialized cardiomyocyte readily identified in culture [11]. Consistent with this explanation, the duration of the events in Figs. 3(c) (0.5 s) and (d) (0.4 s) are similar.

In summary, we have demonstrated a fiber-optic SD-DIC microscope for imaging both reflective surfaces and live cells and for monitoring dynamics at selected sample sites. SD-DIC offers a means to quantitatively decouple OPL gradient and intensity in a single measurement with high sensitivity. The proposed SD-DIC is a point-scanning system and as such achieves enhanced OPL gradient resolution at the expense of acquisition speed. Using existing technologies, the system can be adapted to achieve approximately 1 Hz per frame for two-dimensional imaging and greater than 10 kHz for single-point measurements. Hence, wide-field imaging using SD-DIC is most suited for high-resolution, low-speed characterization, such as surface profiling or relatively slow dynamics (on the order of a few seconds) of live biological specimens, while fast dynamics below 0.1 ms can be monitored for a selected location.

This work is supported by the National Institutes of Health (NIH) (National Cancer Institute) R01CA138594, and National Science Foundation (NSF) under grants CBET-0651622 and MRI-1039562. N. T. Shaked gratefully acknowledges the support of the Bikura Postdoctoral Fellowship from Israel.

References

1. M. G. Nomarski, *J. Phys. Radium* **16**, S9 (1955).
2. S. V. King, A. Libertun, R. Piestun, C. J. Cogswell, and C. Preza, *J. Biomed. Opt.* **13**, 024020 (2008).
3. B. Heise and D. Stifter, *Opt. Lett.* **34**, 1306 (2009).
4. D. Fu, S. Oh, W. Choi, T. Yamauchi, A. Dorn, Z. Yaqoob, R. R. Dasari, and M. S. Feld, *Opt. Lett.* **35**, 2370 (2010).
5. M. R. Arnison, K. G. Larkin, C. J. R. Sheppard, N. I. Smith, and C. J. Cogswell, *J. Microsc. (Oxford)* **214**, 7 (2004).
6. M. A. Choma, M. V. Sarunic, C. H. Yang, and J. A. Izatt, *Opt. Express* **11**, 2183 (2003).
7. M. A. Choma, A. K. Ellerbee, C. H. Yang, T. L. Creazzo, and J. A. Izatt, *Opt. Lett.* **30**, 1162 (2005).
8. J. Zhang, B. Rao, L. F. Yu, and Z. P. Chen, *Opt. Lett.* **34**, 3442 (2009).
9. C. K. Hitznerberger and A. F. Fercher, *Opt. Lett.* **24**, 622 (1999).
10. N. T. Shaked, L. L. Satterwhite, N. Bursac, and A. Wax, *Opt. Express* **1**, 706 (2010).
11. T. Korhonen, S. L. Hanninen, and P. Tavi, *Biophys. J.* **96**, 1189 (2009).